INTERNATIONAL JOURNAL FOR NUMERICAL METHODS IN FLUIDS
Int. J. Numer. Meth. Fluids 2011; **00**:1–24 *Prepared using* fldauth.cls *[Version: 2002/09/18 v1.01]*

On the Pressure Approximation in Nonstationary Incompressible Flow Simulations on Dynamically Varying Spatial Meshes

Michael Besier*, Winnifried Wollner

Department of Applied Mathematics, University of Heidelberg, Im Neuenheimer Feld 293/294, 69120 Heidelberg, Germany

SUMMARY

Subject of this paper is a defect in the approximation of the pressure on dynamically changing spatial meshes in the computation of nonstationary incompressible flows. The observed behavior is due to the fact that discrete solenoidal fields lose this property under changes of the spatial discretization. This phenomenon is analyzed for discontinuous Galerkin finite element discretizations in time and possible ways are considered to circumvent this problem. Copyright © 2011 John Wiley & Sons, Ltd.

KEY WORDS: incompressible Navier-Stokes equations, space-time finite elements, dynamically changing meshes, pressure approximation, backward Euler scheme, discontinuous Galerkin method in time

1. INTRODUCTION

The computational costs for the numerical solution of nonstationary flow problems are comparatively high due to the complex structure of such problems, especially when dealing with three-dimensional geometries. Thus, it is crucial to apply adaptive refinement techniques to reduce the size of the approximative problem without reducing the accuracy of the approximation. To be most efficient in capturing the dynamics of a nonstationary flow problem, it is desirable to use so-called *dynamic meshes* for the discretization in space. That is, one uses possibly different meshes at different time points. In this way, one can efficiently resolve and track layers marching through the domain, for example. However, by doing so one will usually obtain pressure approximations that diverge when the size of the time step is reduced. In contrast, this behavior is not observed when one is concerned with the approximation of the velocities.

To illustrate this defect, we consider the benchmark configuration "Laminar Flow Around a Cylinder", see, e. g., [1] or Section 3 for a precise description of the setting. Figure 1 shows the temporal evolution of the lift-coefficient. These values were obtained using a spatial

*Correspondence to: Michael Besier, Department of Applied Mathematics, University of Heidelberg, Im Neuenheimer Feld 293/294, 69120 Heidelberg, Germany

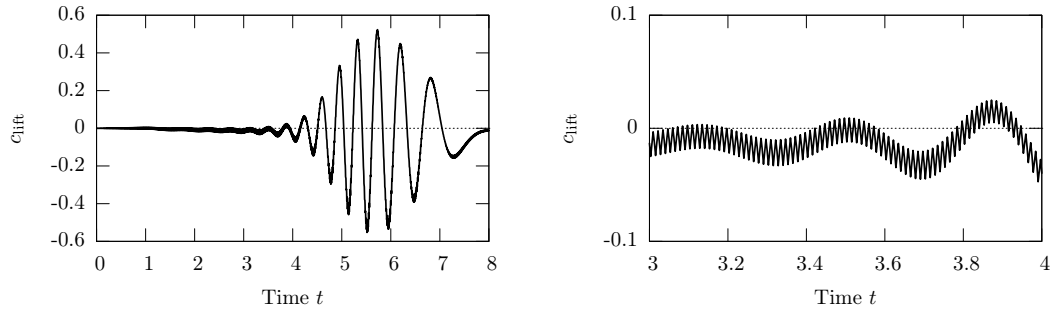

Figure 1: Temporal evolution of the lift-coefficient c_{lift} for the benchmark "Laminar Flow Around a Cylinder" on an oscillating spatial mesh in time

discretization in which the mesh was changed every second time step in order to show the potentially disastrous effects of this defect. We observe oscillations, especially in the right picture which shows a closer look at the subinterval $[3, 4]$. It is clear that such a behavior is undesirable if one is concerned with the determination of pressure dependent quantities. It is even more so if refinement in time is stirred by temporal gradients of the pressure. This is particularly due to the fact, that the oscillations are caused by overrefinement in time as we will see in Section 4.

This behavior is striking, in particular as adaptive methods are widely used in the context of finite element discretizations of partial differential equations, see, for example, [2] or [3] for an overview. Applications to nonstationary incompressible flow problems can be found, e. g., in [4], [5], or [6, 7]. However, while the usage of dynamically changing spatial meshes seems straight forward in the context of Galerkin finite element discretizations, there are some pitfalls if one is interested in the approximation of the pressure as mentioned before. The aim of this paper is to describe and analyze this defect and to present a way to circumvent it. These results are based on the PhD thesis of the first author, see [7].

In what follows, we consider nonstationary incompressible flows described by the Navier-Stokes equations, given in the form

$$\begin{aligned} \partial_t \boldsymbol{v} - \nu \Delta \boldsymbol{v} + (\boldsymbol{v} \cdot \nabla)\boldsymbol{v} + \nabla p &= \boldsymbol{f} && \text{in } I \times \Omega, \\ \nabla \cdot \boldsymbol{v} &= 0 && \text{in } I \times \Omega, \\ \boldsymbol{v}(0) &= \boldsymbol{v^0} && \text{in } \Omega \end{aligned} \tag{1.1}$$

with a time interval $I = (0, T)$, computational domain $\Omega \subseteq \mathbb{R}^d$, $d \in \{ 2, 3 \}$, kinematic viscosity ν, volume forces $\boldsymbol{f}$, and initial values $\boldsymbol{v^0}$. These equations have to be supplemented by appropriate boundary conditions. For sake of simplicity, we consider no-slip Dirichlet boundary conditions.

The discretization of the nonstationary incompressible Navier-Stokes equations (1.1) is done by means of space-time finite element methods. To do so, we state the variational formulation of (1.1) which reads as follows: For given $\boldsymbol{f} \in L^2(I, H^{-1}(\Omega)^d)$ and $\boldsymbol{v^0} \in L^2(\Omega)^d$ find

$\boldsymbol{u} \coloneqq (\boldsymbol{v}, p)^T \in X$ such that

$$\int_I \big\{(\partial_t \boldsymbol{v}, \boldsymbol{\psi}) + \nu(\nabla \boldsymbol{v}, \nabla \boldsymbol{\psi}) + ((\boldsymbol{v} \cdot \nabla)\boldsymbol{v}, \boldsymbol{\psi}) - (p, \nabla \cdot \boldsymbol{\psi}) + (\nabla \cdot \boldsymbol{v}, \chi)\big\}\ \mathrm{d}t \\ + (\boldsymbol{v}(0) - \boldsymbol{v^0}, \boldsymbol{\psi}(0)) = \int_I (\boldsymbol{f}, \boldsymbol{\psi})\ \mathrm{d}t \quad \forall \boldsymbol{\varphi} \coloneqq (\boldsymbol{\psi}, \chi)^T \in X, \quad (1.2)$$

where $(\cdot, \cdot)$ denotes the inner product on $L^2(\Omega)$ (or $L^2(\Omega)^d$) and the space X is given as

$$X \coloneqq \Big\{ \boldsymbol{u} = (\boldsymbol{v}, p)^T \ \Big|\ \boldsymbol{v} \in L^2(I, H_0^1(\Omega)^d),\ \partial_t \boldsymbol{v} \in L^2(I, H^{-1}(\Omega)^d),\ p \in L^2(I, L^2(\Omega)/\mathbb{R}) \Big\}.$$

For questions on existence and uniqueness of solutions, we refer to [8].

The rest of this paper is structured as follows. In Section 2, we start with the discretization of the nonstationary Navier-Stokes equations. Then, in Section 3, we consider a well known benchmark problem to illustrate the behavior of the pressure once the spatial discretization is changed over time. That section concludes by stating a model problem that exhibits the same behavior, thereby showing, that the defect is not caused by the nonlinearity or the time dependent data in the benchmark configuration. In Section 4, we analyze the behavior both numerically as well as analytically. Finally, in Section 5, we demonstrate how the problem can be circumvented.

2. DISCRETIZATION

In this section, we describe the discretization of the weak formulation of the time-dependent incompressible Navier-Stokes equations (1.2). The discretization in space as well as in time will be done by means of Galerkin finite element methods.

2.1. Discretization in time

For the semi-discretization in time, we use *discontinuous Galerkin* (dG) methods. To this end, we partition the time interval $\bar{I} = [0, T]$ into

$$\bar{I} = \{0\} \cup I_1 \cup \cdots \cup I_m \cup \cdots \cup I_M$$

with subintervals $I_m \coloneqq (t_{m-1}, t_m]$ of length $k_m \coloneqq t_m - t_{m-1}$ using time points

$$0 = t_0 < t_1 < \cdots < t_m < \cdots < t_M = T.$$

The discretization parameter k is given as a piecewise constant function by setting $k\big|_{I_m} \coloneqq k_m$ for $m = 1, \ldots, M$.

The dG(r) semi-discretization of the incompressible Navier-Stokes equations (1.2) then seeks a solution $\boldsymbol{u_k} = (\boldsymbol{v_k}, p_k)^T$ which is piecewise polynomial of degree r on each subinterval I_m. For further details, we refer to [9] or [6, 7].

Remark 2.1. *Due to the discontinuity of the test functions, the dG(r) discretizations decouple into a sequence of time steps. For example, the dG(0) discretization is a variant of the backward Euler method, while the dG(1) discretization, after applying quadrature rules to the temporal integrals, corresponds to some implicit Runge-Kutta method.*

2.2. Discretization in space

For the discretization in space of the semi-discrete problems obtained in the previous subsection, we use *continuous Galerkin* (cG) methods. To this end, we use two- or three-dimensional shape-regular meshes, see, e. g., [10]. A mesh consists of open, non-overlapping elements K, such that $\bigcup \overline{K} = \overline{\Omega} \subseteq \mathbb{R}^d$, $d \in \{ 2, 3 \}$. The corresponding mesh is denoted by $\mathcal{T}_h = \{ K \}$, where the discretization parameter h is defined as a cellwise constant function by setting $h\big|_K = h_K = \operatorname{diam}(K)$. On the mesh $\mathcal{T}_h$, we construct a conforming finite element space $V_h^s \subseteq H^1(\Omega)$ in a standard way:

$$V_h^s \coloneqq \left\{ v \in C(\overline{\Omega}) \;\middle|\; v\big|_K \in \mathcal{Q}_s(K) \text{ for } K \in \mathcal{T}_h \right\},$$

where $\mathcal{Q}_s(K)$ denotes the space of isoparametric finite elements of degree s.

To obtain the formulation of the fully discrete problem, we allow dynamic mesh change in time, but the time steps k_m are kept constant in space. To this end, we associate with each time point t_m a mesh $\mathcal{T}_h^m$ and corresponding (spatial) finite element spaces $V_h^{s_{\boldsymbol{v}},m}$ and $V_h^{s_p,m}$. We then define the following space-time finite element space:

$$\begin{aligned} X_{kh}^{r,s} \coloneqq \Big\{ \boldsymbol{u_{kh}} = (\boldsymbol{v_{kh}}, p_{kh})^T \;\Big|\; & \boldsymbol{v_{kh}}(0) \in (H_h^0)^d,\ \boldsymbol{v_{kh}}\big|_{I_m} \in \mathcal{P}_r(I_m, (H_h^m)^d), \\ & p_{kh}\big|_{I_m} \in \mathcal{P}_r(I_m, L_h^m),\ m = 1, \dots, M \Big\}, \end{aligned}$$

where

$$H_h^m \coloneqq V_h^{s_{\boldsymbol{v}},m} \cap H_0^1(\Omega) \quad \text{and} \quad L_h^m \coloneqq V_h^{s_p,m} \cap L^2(\Omega)/\mathbb{R}.$$

Finally, the fully discrete formulation of problem (1.2) reads: Find $\boldsymbol{u_{kh}} = (\boldsymbol{v_{kh}}, p_{kh})^T \in X_{kh}^{r,s}$ such that

$$\begin{aligned} & \sum_{m=1}^{M} \int_{I_m} \big\{ (\partial_t \boldsymbol{v_{kh}}, \boldsymbol{\psi}) + \nu(\nabla \boldsymbol{v_{kh}}, \nabla \boldsymbol{\psi}) + ((\boldsymbol{v_{kh}} \cdot \nabla)\boldsymbol{v_{kh}}, \boldsymbol{\psi}) \\ & - (p_{kh}, \nabla \cdot \boldsymbol{\psi}) + (\nabla \cdot \boldsymbol{v_{kh}}, \chi) \big\} \,\mathrm{d}t + \sum_{m=0}^{M-1} ([\boldsymbol{v_{kh}}]_m, \boldsymbol{\psi}_m^+) + (\boldsymbol{v}_{\boldsymbol{kh},0}^-, \boldsymbol{\psi}_0^-) \\ & \qquad = \int_I (\boldsymbol{f}, \boldsymbol{\psi}) \,\mathrm{d}t + (\boldsymbol{v^0}, \boldsymbol{\psi}_0^-) \quad \forall \boldsymbol{\varphi} = (\boldsymbol{\psi}, \chi)^T \in X_{kh}^{r,s}, \end{aligned} \tag{2.1}$$

where

$$u_{kh,m}^{\pm} \coloneqq \lim_{\varepsilon \downarrow 0} u_{kh}(t_m \pm \varepsilon), \quad [u_{kh}]_m \coloneqq u_{kh,m}^+ - u_{kh,m}^-$$

denotes the limit "from above" and "from below" at time point t_m as well as the "jump" of discontinuous functions u_{kh}, respectively.

2.3. Stabilization

The fully discrete formulation (2.1) does not lead to a stable approximation of problem (1.2) unless the spatial finite element spaces H_h^m and L_h^m fulfill the Babuška-Brezzi inf-sup-stability condition. This condition states (see, for example, [11]) that there is a constant β independent of h such that

$$\inf_{p_h \in L_h^m} \sup_{\boldsymbol{v_h} \in (H_h^m)^d} \frac{(p_h, \nabla \cdot \boldsymbol{v_h})}{\|p_h\| \|\nabla \boldsymbol{v_h}\|} \geq \beta > 0. \tag{2.2}$$

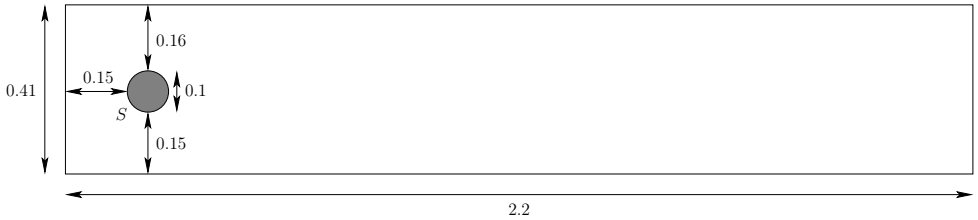

Figure 2: Geometry for the benchmark configuration "Laminar Flow Around a Cylinder"

Especially in cases of equal-order trial spaces, i. e., $s_{\boldsymbol{v}} = s_p = s$, condition (2.2) is not fulfilled in general. To obtain stable approximations, one has to use different finite elements for velocities and pressure such as the Taylor-Hood element ($s_{\boldsymbol{v}} = 2$, $s_p = 1$, for example). For more details on this topic, we refer to [12], [13], or [11]. Alternatively one may add stabilization terms. For implementational reasons, we use equal-order trial spaces for the computation of the benchmark and apply the so-called *local projection stabilization* (LPS), see, e. g., [14, 15].

For the computation of the subsequent examples, we used the two finite element packages deal.II [16] and Gascoigne [17].

3. Problem description and reduction to a model problem

3.1. Description of the problem

In this subsection, we aim at computing the lift-coefficient in the two-dimensional benchmark problem "Laminar Flow Around a Cylinder", see [1] for a detailed description of the configuration. The geometry is depicted in Figure 2.

The time-dependent inflow condition on the left side of the domain is given by

$$v_1(t, \boldsymbol{x}) = \frac{6 \sin(\frac{\pi t}{8})}{(0.41)^2} x_2(0.41 - x_2), \quad v_2(t, \boldsymbol{x}) = 0.$$

On the outflow boundary on the right side of the computational domain, we apply the "do nothing" boundary condition, see [18]. On all other boundaries, we prescribe no-slip Dirichlet boundary conditions. The final time is set to $T = 8$. This setting leads to a Reynolds number $\mathrm{Re}(t) = \frac{\bar{U}(t)D}{\nu}$ based on the mean inflow velocity

$$\bar{U}(t) = \frac{2}{3} v_1(t, 0, 0.205) = \sin\Big(\frac{\pi t}{8}\Big),$$

the viscosity $\nu = 10^{-3}$, and the diameter of the obstacle $D = 0.1$ of $0 \leq \mathrm{Re}(t) \leq 100$ for $t \in I = (0, 8)$.

In this example, we apply the dG(1) discretization in time with the stabilized $\mathcal{Q}_1/\mathcal{Q}_1$ discretization in space. After five iterations of adaptive temporal and spatial refinement using dynamic meshes, following [6, 7], the temporal evolution of the lift-coefficient looks as depicted

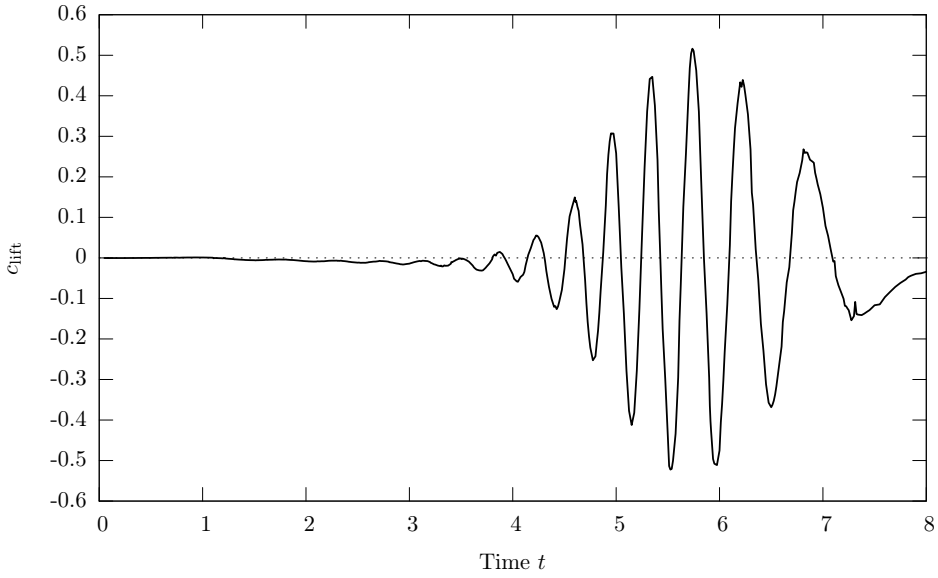

Figure 3: Lift-coefficient c_{lift} after five adaptation cycles using adaptive temporal and spacial meshes (compare Figure 1)

in Figure 3. Here, the lift-coefficient is given as

$$c_{\text{lift}} = -\frac{2}{\bar{U}^2 D} \int_S (\nu \partial_{\boldsymbol{n}} (\boldsymbol{v} \cdot \boldsymbol{t}) n_1 + p n_2) \, \mathrm{d}o,$$

where S denotes the surface of the obstacle, $\boldsymbol{n} = (n_1, n_2)^T$ is the outward unit normal vector on S and $(\boldsymbol{v} \cdot \boldsymbol{t})$ denotes the tangential component of $\boldsymbol{v}$ with unit tangential vector $\boldsymbol{t} = (n_2, -n_1)^T$.

We observe slight oscillations in the lift-coefficient, for example, near $t = 7.25$. However, as indicated in Figure 1 these oscillations can become arbitrarily large, depending on the chosen temporal and spatial discretizations. Further investigations in Section 3.2 show that such oscillations especially occur when switching from one spatial mesh to another. In the following sections, we will numerically analyze these oscillations.

3.2. Reduction to model problem

Let us first show that the arising problems are not related to the time-dependent inflow boundary condition. To this end, we remove the oscillatory sine-term from the inflow condition and reduce the inflow velocity to

$$v_1(t, \boldsymbol{x}) = \frac{1.2}{(0.41)^2} x_2 (0.41 - x_2), \quad v_2(t, \boldsymbol{x}) = 0.$$

This yields a constant Reynolds number of $\mathrm{Re} = 20$ with a stationary solution. Since the effects we want to study can already be seen when working with the simplest temporal discretization, we apply the dG(0) discretization in time which here coincides with the backward Euler

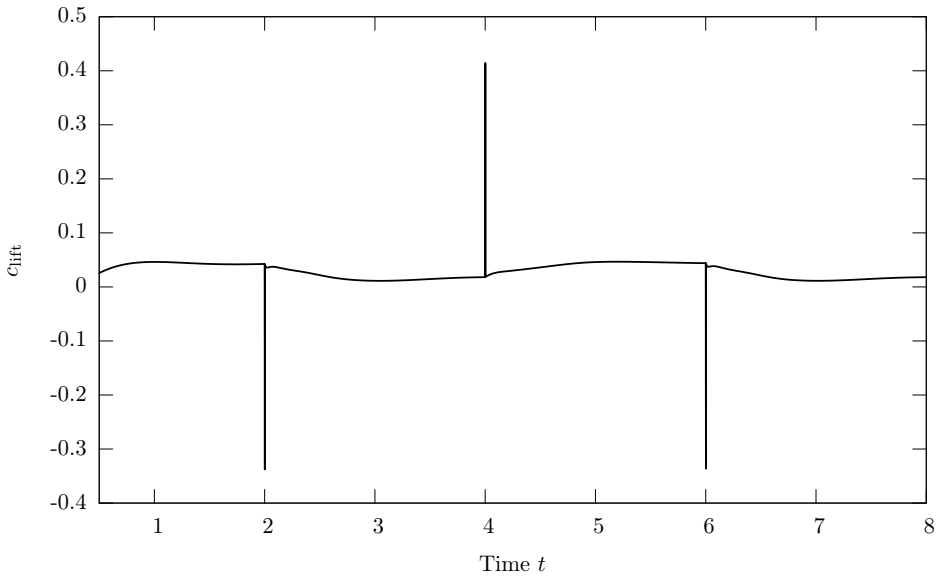

Figure 4: Temporal evolution of the lift-coefficient

scheme. For the discretization in space, we use the stabilized $\mathcal{Q}_1/\mathcal{Q}_1$ discretization. We again focus on computing the lift-coefficient whose reference value in this configuration is given as $c_{\text{lift}}^{(\text{ref})} = 0.010618948146$, see, for example [19].

We use the time interval $I = (0, 8)$ with different spatial meshes. Denoting the meshes on $(2, 4] \cup (6, 8]$ with $\mathcal{T}_h$, we use the mesh $\mathcal{T}_{2h}$ on $[0, 2] \cup (4, 6]$. That is, we perform uniform refinement of the spatial mesh at $t = 2$ and $t = 6$, whereas at $t = 4$ uniform coarsening is applied. The evolution of the lift-coefficient on the time interval $[0.5, 8]$, obtained with a uniform time step size of $k = 1.5625 \cdot 10^{-3}$, is shown in Figure 4. We neglect the beginning of the time interval where a singularity in the pressure evolves for $t \to 0$ due to compatibility conditions that are not fulfilled with the initial condition $\boldsymbol{v}^{\mathbf{0}} = \mathbf{0}$, see, for instance, [20]. The spatial meshes $\mathcal{T}_{2h}$ and $\mathcal{T}_h$ used in these computations are depicted in Figure 5.

We observe that precisely in the first time step on the new mesh the lift-coefficient deteriorates. We also note that these errors are even larger than in the example presented in the previous subsection.

In the remaining part of this section, we will consider the oscillations in the lift-coefficient shown in the last section. We show that they are caused when switching from one spatial mesh to another. These errors are located solely in the discrete pressure and localized to exactly one interval. First we show that this effect can already be observed when solving the linear Stokes equations instead of the nonlinear Navier-Stokes equations. Furthermore, these errors also arise when applying uniform refinement of a mesh. We state a model problem on a polygonally bounded domain in order to avoid special effects from the approximation of a curved boundary.

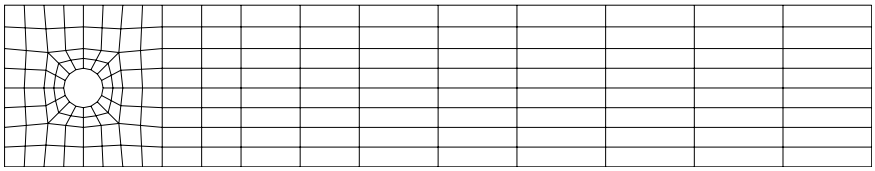

(a) Mesh $\mathcal{T}_{2h}$

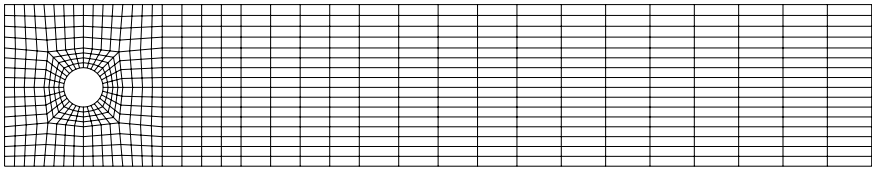

(b) Mesh $\mathcal{T}_h$

Figure 5: Spatial meshes used for the computation of the lift-coefficient

Hence, we want to find $(\boldsymbol{v}, p)^T$ such that

$$\begin{aligned} \partial_t \boldsymbol{v} - \Delta \boldsymbol{v} + \nabla p &= \boldsymbol{f} && \text{in } I \times \Omega, \\ \nabla \cdot \boldsymbol{v} &= 0 && \text{in } I \times \Omega, \\ \boldsymbol{v} &= \boldsymbol{0} && \text{in } \{\, 0 \,\} \times \Omega, \\ \boldsymbol{v} &= \boldsymbol{0} && \text{on } I \times \partial\Omega. \end{aligned} \tag{3.1}$$

Here, we choose $I = (0, 9)$ and $\Omega = (-1, 1)^2$. Let $\boldsymbol{f}$ be given in such a way that (3.1) possesses the stationary limit

$$\begin{aligned} \overline{\boldsymbol{v}}(\boldsymbol{x}) &= \begin{pmatrix} \cos^2(\frac{\pi x_1}{2}) \cos(\frac{\pi x_2}{2}) \sin(\frac{\pi x_2}{2}) \\ -\cos(\frac{\pi x_1}{2}) \sin(\frac{\pi x_1}{2}) \cos^2(\frac{\pi x_2}{2}) \end{pmatrix}, \\ \overline{p}(\boldsymbol{x}) &= \cos(\tfrac{\pi x_1}{2}) \sin(\tfrac{\pi x_1}{2}) \cos(\tfrac{\pi x_2}{2}) \sin(\tfrac{\pi x_2}{2}). \end{aligned}$$

We subdivide $\bar{I} = I^{(1)} \cup I^{(2)} \cup I^{(3)}$ with

$$I^{(1)} = [0, 3], \quad I^{(2)} = (3, 6], \quad I^{(3)} = (6, 9].$$

On $I^{(1)}$ and $I^{(3)}$, we use a uniform spatial mesh of cell size $2h$, whereas on the subinterval $I^{(2)}$ a uniform spatial mesh of cell size h is used. That is, we switch the spatial mesh uniformly from $2h$ to h at $t = 3$ and from h to $2h$ at $t = 6$. The subintervals are chosen long enough for the discrete solution to reach the stationary limit on each mesh.

The errors $\|\nabla(\overline{\boldsymbol{v}} - \boldsymbol{v_{kh}})\|$ and $\|\overline{p} - p_{kh}\|$ for a uniform step size of $k \approx 2 \cdot 10^{-4}$ and mesh size $h = 2^{-4}$ are shown in Figure 6. As we can see, both the velocity and the pressure approximation show a transient phenomenon when switching the spatial mesh. However, while the approximation of the velocity component is quite satisfactory, the transient phenomenon in the pressure component is superposed by an additional error which causes the approximation of the pressure to deteriorate under a change of the spatial mesh, see Figure 7.

In the next section, we will further analyze how these errors behave under systematic refinement of the temporal and spatial discretization.

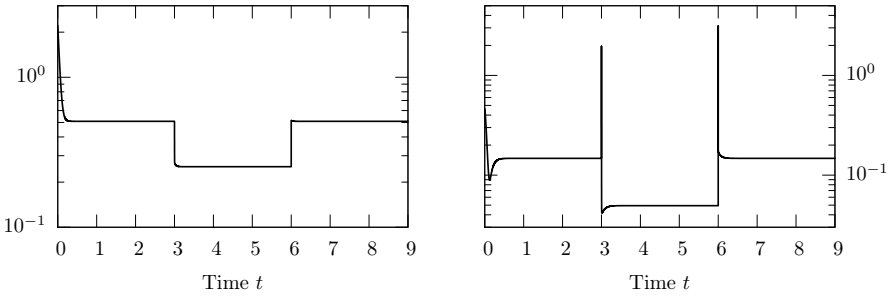

Figure 6: Errors $\|\nabla(\overline{\boldsymbol{v}} - \boldsymbol{v_{kh}})\|$ (left) and $\|\overline{p} - p_{kh}\|$ (right)

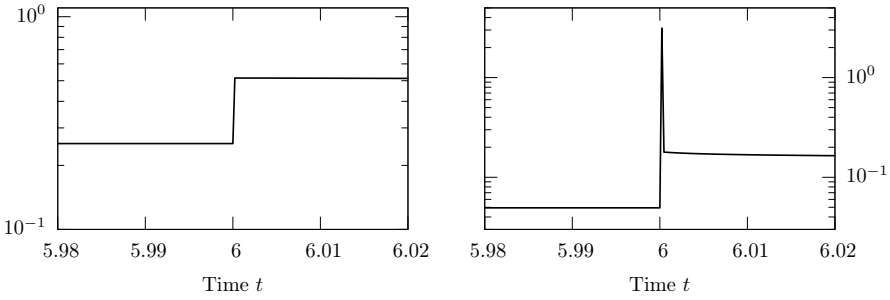

Figure 7: Errors $\|\nabla(\overline{\boldsymbol{v}} - \boldsymbol{v_{kh}})\|$ (left) and $\|\overline{p} - p_{kh}\|$ (right) near $t = 6$

4. ANALYSIS OF THE PROBLEM

4.1. Behavior of the error under temporal and spatial refinement

In this subsection, we numerically analyze the behavior of the error described in the last section. We especially consider systematic uniform refinement of the temporal and spatial discretization. The analysis will be done by means of the model problem presented in the previous section. We are going to consider the equal-order $\mathcal{Q}_1/\mathcal{Q}_1$ and $\mathcal{Q}_2/\mathcal{Q}_2$ discretizations in space together with the local projection stabilization as well as the inf-sup-stable $\mathcal{Q}_2/\mathcal{Q}_1$-Taylor-Hood element (see, for instance, [12]). For the temporal discretization we will apply the dG(0) and dG(1) method as well as the fractional-step-θ scheme, which is a popular time-stepping scheme often used in computational fluid dynamics, see [21], [22], [23] or [24, 25]. For convenience of the reader, we briefly recall the precise form of the fractional-step-θ scheme: Let the parameters

$$\theta = 1 - \frac{1}{2}\sqrt{2}, \quad \theta' = 1 - 2\theta, \quad \alpha = \frac{\theta'}{1-\theta}, \quad \beta = 1 - \alpha$$

be given. Then one fractional-step-θ time step $(\boldsymbol{V_{m-1}}, P_{m-1})^T \rightarrow (\boldsymbol{V_m}, P_m)^T$ for the incompressible Navier-Stokes equations consists of the following three sub-steps $t_{m-1} \rightarrow t_{m-1+\theta} \rightarrow t_{m-\theta} \rightarrow t_m$ (where the equations should be fulfilled for all $\boldsymbol{\varphi} = (\boldsymbol{\psi}, \chi)^T \in$

$(H_h^m)^d \times L_h^m$):

$$
\begin{aligned}
(\boldsymbol{V_{m-1+\theta}}, \boldsymbol{\psi}) + \alpha\theta k_m \big\{ \nu(\nabla \boldsymbol{V_{m-1+\theta}}, \nabla \boldsymbol{\psi}) + ((\boldsymbol{V_{m-1+\theta}} \cdot \nabla)\boldsymbol{V_{m-1+\theta}}, \boldsymbol{\psi}) \big\} \\
+ \theta k_m (P_{m-1+\theta}, \nabla \cdot \boldsymbol{\psi}) = (\boldsymbol{V_{m-1}}, \boldsymbol{\psi}) - \beta\theta k_m \big\{ \nu(\nabla \boldsymbol{V_{m-1}}, \nabla \boldsymbol{\psi}) \\
+ ((\boldsymbol{V_{m-1}} \cdot \nabla)\boldsymbol{V_{m-1}}, \boldsymbol{\psi}) \big\} + \theta k_m (\boldsymbol{f_{m-1}}, \boldsymbol{\psi}) \\
(\nabla \cdot \boldsymbol{V_{m-1+\theta}}, \chi) = 0
\end{aligned}
$$

$$
\begin{aligned}
(\boldsymbol{V_{m-\theta}}, \boldsymbol{\psi}) + \beta\theta' k_m \big\{ \nu(\nabla \boldsymbol{V_{m-\theta}}, \nabla \boldsymbol{\psi}) + ((\boldsymbol{V_{m-\theta}} \cdot \nabla)\boldsymbol{V_{m-\theta}}, \boldsymbol{\psi}) \big\} \\
+ \theta' k_m (P_{m-\theta}, \nabla \cdot \boldsymbol{\psi}) = (\boldsymbol{V_{m-1+\theta}}, \boldsymbol{\psi}) - \alpha\theta' k_m \big\{ \nu(\nabla \boldsymbol{V_{m-1+\theta}}, \nabla \boldsymbol{\psi}) \\
+ ((\boldsymbol{V_{m-1+\theta}} \cdot \nabla)\boldsymbol{V_{m-1+\theta}}, \boldsymbol{\psi}) \big\} + \theta' k_m (\boldsymbol{f_{m-\theta}}, \boldsymbol{\psi}) \\
(\nabla \cdot \boldsymbol{V_{m-\theta}}, \chi) = 0
\end{aligned}
$$

$$
\begin{aligned}
(\boldsymbol{V_m}, \boldsymbol{\psi}) + \alpha\theta k_m \big\{ \nu(\nabla \boldsymbol{V_m}, \nabla \boldsymbol{\psi}) + ((\boldsymbol{V_m} \cdot \nabla)\boldsymbol{V_m}, \boldsymbol{\psi}) \big\} \\
+ \theta k_m (P_m, \nabla \cdot \boldsymbol{\psi}) = (\boldsymbol{V_{m-\theta}}, \boldsymbol{\psi}) - \beta\theta k_m \big\{ \nu(\nabla \boldsymbol{V_{m-\theta}}, \nabla \boldsymbol{\psi}) \\
+ ((\boldsymbol{V_{m-\theta}} \cdot \nabla)\boldsymbol{V_{m-\theta}}, \boldsymbol{\psi}) \big\} + \theta k_m (\boldsymbol{f_{m-\theta}}, \boldsymbol{\psi}) \\
(\nabla \cdot \boldsymbol{V_m}, \chi) = 0
\end{aligned}
$$

For simplicity, we have omitted terms arising from stabilization.

In what follows, the behavior of the error in the pressure under systematic uniform refinement of the spatial or the temporal discretization is studied for different spatial and temporal discretizations. Since the error is concentrated to the first time step on a new mesh, we especially focus on its development there.

4.1.1. Spatial refinement This subsection is dedicated to the numerical analysis of the error in the pressure under uniform refinement of the spatial discretization. To this end, we fix the temporal discretization with a uniform time step size of $k = 3 \cdot 10^{-2}$. As mentioned in the previous section, we use the mesh $\mathcal{T}_{2h}$ on $I^{(1)}$ and $I^{(3)}$, whereas on $I^{(2)}$ the mesh $\mathcal{T}_h$ is used. We study the development of the error in the pressure component for $h \to 0$.

The numerical order of convergence of $\|\overline{p} - p_{kh}\|$ obtained after four uniform refinements of the spatial meshes starting with $h = \frac{1}{4}$ is given in Table I. We can conclude that the error in the pressure component in the first time step on a new spatial mesh converges for $h \to 0$ (at least) with the same order as the overall spatial discretization error.

4.1.2. Temporal refinement In this subsection, the development of the pressure error under systematic uniform refinement of the temporal discretization is considered, that is we consider the case $k \to 0$. To this end, we fix the spatial discretization with $h = \frac{1}{16}$.

The numerical order of convergence of $\|\overline{p} - p_{kh}\|$ obtained by uniform refinement of the time step size, starting with $k = 1.875 \cdot 10^{-3}$, is given in Table II.

We observe that under uniform refinement of the temporal discretization the error in the pressure component when uniformly refining the spatial mesh increases like $O(k^{-1})$ for the dG(0) and the dG(1) discretization whereas for the fractional-step-θ scheme this error is almost

Table I: Order of convergence of $\|\overline{p} - p_{kh}\|$ under spatial refinement with fixed time step size $k = 3 \cdot 10^{-2}$ with different spatial and temporal discretizations at the mesh directly following the change of the spatial meshes

	dG(0)		dG(1)		fractional-step-θ	
	$t = 3 + k$	$t = 6 + k$	$t = 3 + k$	$t = 6 + k$	$t = 3 + k$	$t = 6 + k$
$\mathcal{Q}_1/\mathcal{Q}_1$	1.66	1.70	1.38	1.49	1.38	1.60
$\mathcal{Q}_2/\mathcal{Q}_2$	2.02	2.00	2.07	2.00	2.06	2.00
$\mathcal{Q}_2/\mathcal{Q}_1$	2.04	2.03	2.15	2.02	2.06	2.02

Table II: Order of convergence of $\|\overline{p} - p_{kh}\|$ under temporal refinement with fixed spatial mesh size $h = \frac{1}{16}$ with different spatial and temporal discretizations at the mesh directly following the change of the spatial meshes

	dG(0)		dG(1)		fractional-step-θ	
	$t = 3 + k$	$t = 6 + k$	$t = 3 + k$	$t = 6 + k$	$t = 3 + k$	$t = 6 + k$
$\mathcal{Q}_1/\mathcal{Q}_1$	−0.94	−0.95	−0.99	−1.03	−0.22	0.00
$\mathcal{Q}_2/\mathcal{Q}_2$	−0.96	−0.92	−1.02	−1.03	−0.14	−0.06
$\mathcal{Q}_2/\mathcal{Q}_1$	−0.96	−0.92	−1.01	−1.03	−0.15	−0.07

independent of k. The reason for this behavior of the fractional-step-θ scheme will be clarified in Remark 5.1. For uniform coarsening of the spatial mesh we observe the same behavior.

Since the support of this error is exactly one time step, this shows the behavior of a Dirac approximation and hence the error, for example, in mean functional values involving the pressure, does not vanish for $k \to 0$ unless $h \to 0$ sufficiently fast (compare Section 4.1.1).

4.2. Theoretical investigation

This section presents a theoretical investigation of the behavior of the pressure approximation when switching the spatial mesh. To this end, we consider the inf-sup-stable $\mathcal{Q}_2/\mathcal{Q}_1$-Taylor-Hood element for the spatial discretization in combination with the backward Euler time-stepping scheme. As our numerical results indicate it will be sufficient to consider one step of the backward Euler method (e. g., the dG(0) time discretization) during which the spatial discretization is changed to explain the undesired behavior of the pressure. As in the previous subsections, we consider uniform refinement or coarsening of a uniform mesh. Furthermore, we assume the domain $\Omega \subseteq \mathbb{R}^d$, $d \in \{ 2, 3 \}$, to be bounded, polygonal and convex.

Let $(\boldsymbol{v}, p)^T \in H_0^1(\Omega)^d \times L^2(\Omega)/\mathbb{R}$ be the unique solution of the stationary Stokes problem for $\mathrm{Re} = 1$:

$$\begin{aligned} (\nabla \boldsymbol{v}, \nabla \boldsymbol{\psi}) - (p, \nabla \cdot \boldsymbol{\psi}) &= (\boldsymbol{f}, \boldsymbol{\psi}) \qquad && \forall \boldsymbol{\psi} \in H_0^1(\Omega)^d, \\ (\nabla \cdot \boldsymbol{v}, \chi) &= 0 && \forall \chi \in L^2(\Omega)/\mathbb{R}. \end{aligned} \tag{4.1}$$

Then, this solution also satisfies $(\boldsymbol{v}, p)^T \in H^2(\Omega)^d \times H^1(\Omega)$ as well as the a priori estimate

$$\|\boldsymbol{v}\|_{H^2(\Omega)} + \|p\|_{H^1} \leq C \|\boldsymbol{f}\|, \tag{4.2}$$

see [26] and [27].

Let a uniform decomposition $\mathcal{T}_H$ of $\Omega \subseteq \mathbb{R}^d$ into cells be given. We define the following conforming finite element spaces for the Taylor-Hood element:

$$H_H \coloneqq \left\{ v_H \in C(\overline{\Omega}) \;\middle|\; v_H\big|_K \in \mathcal{Q}_2(K) \;\forall K \in \mathcal{T}_H \right\} \cap H_0^1(\Omega),$$
$$L_H \coloneqq \left\{ p_H \in C(\overline{\Omega}) \;\middle|\; p_H\big|_K \in \mathcal{Q}_1(K) \;\forall K \in \mathcal{T}_H \right\} \cap L^2(\Omega)/\mathbb{R}.$$

Let $(\boldsymbol{v_H}, p_H)^T \in H_H^d \times L_H$ be the approximate solution on the mesh $\mathcal{T}_H$, that is

$$\begin{aligned} (\nabla \boldsymbol{v_H}, \nabla \boldsymbol{\psi}) - (p_H, \nabla \cdot \boldsymbol{\psi}) &= (\boldsymbol{f}, \boldsymbol{\psi}) && \forall \boldsymbol{\psi} \in H_H^d, \\ (\nabla \cdot \boldsymbol{v_H}, \chi) &= 0 && \forall \chi \in L_H. \end{aligned} \tag{4.3}$$

Uniformly refining or coarsening the mesh $\mathcal{T}_H$ yields a spatial mesh $\mathcal{T}_h$ and the corresponding finite element spaces

$$H_h \coloneqq \left\{ v_h \in C(\overline{\Omega}) \;\middle|\; v_h\big|_K \in \mathcal{Q}_2(K) \;\forall K \in \mathcal{T}_h \right\} \cap H_0^1(\Omega),$$
$$L_h \coloneqq \left\{ p_h \in C(\overline{\Omega}) \;\middle|\; p_h\big|_K \in \mathcal{Q}_1(K) \;\forall K \in \mathcal{T}_h \right\} \cap L^2(\Omega)/\mathbb{R}.$$

We note that in contrast to the previous section, we symbolize the difference between the spatial discretizations on the two considered time points by the subscripts H and h rather than by the superscript, e.g., here, we consider H_H and H_h instead of H_h^{m-1} and H_h^m.

Performing one backward Euler step with step size k seeks the solution $(\boldsymbol{v_h^k}, p_h^k)^T \in H_h^d \times L_h$ of

$$\begin{aligned} k^{-1}(\boldsymbol{v_h^k}, \boldsymbol{\psi}) + (\nabla \boldsymbol{v_h^k}, \nabla \boldsymbol{\psi}) - (p_h^k, \nabla \cdot \boldsymbol{\psi}) &= k^{-1}(\boldsymbol{v_H}, \boldsymbol{\psi}) + (\boldsymbol{f}, \boldsymbol{\psi}) && \forall \boldsymbol{\psi} \in H_h^d, \\ (\nabla \cdot \boldsymbol{v_h^k}, \chi) &= 0 && \forall \chi \in L_h. \end{aligned} \tag{4.4}$$

Using the H-projection $\widetilde{\boldsymbol{P}}_{\boldsymbol{h}} \boldsymbol{v_H}$ of $\boldsymbol{v_H}$ into H_h^d as initial value in the backward Euler step, yields the solution $(\hat{\boldsymbol{v}}_{\boldsymbol{h}}^{\boldsymbol{k}}, \hat{p}_h^k)^T \in H_h^d \times L_h$ of

$$\begin{aligned} k^{-1}(\hat{\boldsymbol{v}}_{\boldsymbol{h}}^{\boldsymbol{k}}, \boldsymbol{\psi}) + (\nabla \hat{\boldsymbol{v}}_{\boldsymbol{h}}^{\boldsymbol{k}}, \nabla \boldsymbol{\psi}) - (\hat{p}_h^k, \nabla \cdot \boldsymbol{\psi}) &= k^{-1}(\widetilde{\boldsymbol{P}}_{\boldsymbol{h}} \boldsymbol{v_H}, \boldsymbol{\psi}) + (\boldsymbol{f}, \boldsymbol{\psi}) && \forall \boldsymbol{\psi} \in H_h^d, \\ (\nabla \cdot \hat{\boldsymbol{v}}_{\boldsymbol{h}}^{\boldsymbol{k}}, \chi) &= 0 && \forall \chi \in L_h. \end{aligned} \tag{4.5}$$

Here, $\widetilde{\boldsymbol{P}}_{\boldsymbol{h}} \boldsymbol{v_H}$ is given as the first component of the solution $(\widetilde{\boldsymbol{P}}_{\boldsymbol{h}} \boldsymbol{v_H}, \tilde{p}_h^H)^T \in H_h^d \times L_h$ of

$$\begin{aligned} (\widetilde{\boldsymbol{P}}_{\boldsymbol{h}} \boldsymbol{v_H}, \boldsymbol{\psi}) - (\tilde{p}_h^H, \nabla \cdot \boldsymbol{\psi}) &= (\boldsymbol{v_H}, \boldsymbol{\psi}) && \forall \boldsymbol{\psi} \in H_h^d, \\ (\nabla \cdot \widetilde{\boldsymbol{P}}_{\boldsymbol{h}} \boldsymbol{v_H}, \chi) &= 0 && \forall \chi \in L_h. \end{aligned} \tag{4.6}$$

It is clear that $\|\widetilde{\boldsymbol{P}}_{\boldsymbol{h}}\|_{L(L^2,L^2)} = 1$ by construction, i. e., for any $\boldsymbol{v} \in L^2(\Omega)^d$ it holds $\|\widetilde{\boldsymbol{P}}_{\boldsymbol{h}} \boldsymbol{v}\| \leq \|\boldsymbol{v}\|$.

Lemma 4.1. *The functions $\boldsymbol{v_h^k}$ defined by (4.4) and $\hat{\boldsymbol{v}}_{\boldsymbol{h}}^{\boldsymbol{k}}$ defined by (4.5) coincide. Further, there exists a function $\boldsymbol{v_h^0} \in H_h^d$ and a sequence $k \to 0$ such that the sequence $\boldsymbol{v_h^k}$ fulfills*

$$\|\boldsymbol{v_h^k} - \boldsymbol{v_h^0}\| \to 0 \quad (k \to 0).$$

Proof. If we subtract equation (4.5) from (4.4), we obtain for arbitrary $(\boldsymbol{\psi}, \chi)^T \in H_h^d \times L_h$

$$\begin{aligned} k^{-1}(\boldsymbol{v_h^k} - \hat{\boldsymbol{v}}_{\boldsymbol{h}}^{\boldsymbol{k}}, \boldsymbol{\psi}) + (\nabla(\boldsymbol{v_h^k} - \hat{\boldsymbol{v}}_{\boldsymbol{h}}^{\boldsymbol{k}}), \nabla\boldsymbol{\psi}) - (p_h^k - \hat{p}_h^k, \nabla\cdot\boldsymbol{\psi}) &= -k^{-1}(\tilde{p}_h^H, \nabla\cdot\boldsymbol{\psi}), \\ (\nabla\cdot(\boldsymbol{v_h^k} - \hat{\boldsymbol{v}}_{\boldsymbol{h}}^{\boldsymbol{k}}), \chi) &= 0, \end{aligned} \tag{4.7}$$

where we have applied (4.6) to obtain the right-hand side. Testing (4.7) with $\boldsymbol{\psi} = \boldsymbol{v_h^k} - \hat{\boldsymbol{v}}_{\boldsymbol{h}}^{\boldsymbol{k}} \in H_h^d$ and $\chi = p_h^k - \hat{p}_h^k$ leads to

$$k^{-1}\|\boldsymbol{v_h^k} - \hat{\boldsymbol{v}}_{\boldsymbol{h}}^{\boldsymbol{k}}\|^2 + \|\nabla(\boldsymbol{v_h^k} - \hat{\boldsymbol{v}}_{\boldsymbol{h}}^{\boldsymbol{k}})\|^2 = 0,$$

where the other terms cancel out due to the second equation of (4.7). Hence, we have $\boldsymbol{v_h^k} = \hat{\boldsymbol{v}}_{\boldsymbol{h}}^{\boldsymbol{k}}$.

When testing equation (4.4) with $\boldsymbol{\psi} = \boldsymbol{v_h^k}$ and $\chi = p_h^k$, we obtain

$$k^{-1}\|\boldsymbol{v_h^k}\|^2 + \|\nabla\boldsymbol{v_h^k}\|^2 = k^{-1}(\boldsymbol{v_H}, \boldsymbol{v_h^k}) + (\boldsymbol{f}, \boldsymbol{v_h^k})$$

and hence

$$\|\boldsymbol{v_h^k}\| \le \|\boldsymbol{v_H}\| + k\|\boldsymbol{f}\|.$$

Since $\boldsymbol{v_H}$ and $\boldsymbol{f}$ do not depend on time, we conclude that $\|\boldsymbol{v_h^k}\|$ remains bounded for $k \to 0$. Hence, there is at least one sequence $k \to 0$ and a function $\boldsymbol{v_h^0} \in H_h^d$ such that

$$\|\boldsymbol{v_h^k} - \boldsymbol{v_h^0}\| \to 0 \quad (k \to 0).$$

□

Since H_h^d is finite dimensional, $\boldsymbol{v_h^k}$ converges to $\boldsymbol{v_h^0}$ in every norm, even point-wise. For the following, we define the L^2-projection $\boldsymbol{P_h}\colon L^2(\Omega)^d \to H_h^d$ as usual by

$$(\boldsymbol{P_h v}, \boldsymbol{\psi}) = (\boldsymbol{v}, \boldsymbol{\psi}) \quad \forall \boldsymbol{\psi} \in H_h^d.$$

We are now prepared to proof the observed divergence of the pressure as $k \to 0$.

Lemma 4.2. *The function $\boldsymbol{v_h^0} \in H_h^d$ given by Lemma 4.1 is uniquely determined by $\boldsymbol{v_h^0} = \widetilde{\boldsymbol{P}}_{\boldsymbol{h}}\boldsymbol{v_H}$. Let $p_h^k \in L_h$ be given by* (4.4)*, then either*

$$a)\ \widetilde{\boldsymbol{P}}_{\boldsymbol{h}}\boldsymbol{v_H} = \boldsymbol{P_h v_H} \quad or \quad b)\ \|p_h^k\| \ge C(h)k^{-1}$$

with some constant $C(h) > 0$ independent of k.

Proof. Let $\boldsymbol{v_h^0} \in H_h^d$ and $k \to 0$ be any sequence such that $\boldsymbol{v_h^k} \to \boldsymbol{v_h^0}$, the existence of such objects is ensured by Lemma 4.1.

We note that (4.4) is equivalent to the algebraic system

$$\begin{pmatrix} \boldsymbol{M} + k\boldsymbol{A} & k\boldsymbol{B} \\ -\boldsymbol{B}^T & 0 \end{pmatrix} \begin{pmatrix} \boldsymbol{x^k} \\ \boldsymbol{y^k} \end{pmatrix} = \begin{pmatrix} \boldsymbol{b^k} \\ 0 \end{pmatrix} \tag{4.8}$$

with

$$\boldsymbol{M} = \big((\boldsymbol{\psi_j}, \boldsymbol{\psi_i})\big)_{i,j=1,\dots,N_H}, \quad \boldsymbol{A} = \big((\nabla\boldsymbol{\psi_j}, \nabla\boldsymbol{\psi_i})\big)_{i,j=1,\dots,N_H},$$
$$\boldsymbol{B} = \big(-(\chi_j, \nabla\cdot\boldsymbol{\psi_i})\big)_{\substack{i=1,\dots,N_H,\\ j=1,\dots,N_L}}$$

and right-hand side

$$\boldsymbol{b^k} = \big((\boldsymbol{v_H}, \boldsymbol{\psi_i}) + k(\boldsymbol{f}, \boldsymbol{\psi_i})\big)_{i=1,\dots,N_H}$$

where we use the representations

$$\boldsymbol{v_h^k} = \sum_{j=1}^{N_H} x_j^k \boldsymbol{\psi_j} \quad \text{and} \quad p_h^k = \sum_{j=1}^{N_L} y_j^k \chi_j.$$

Here, $\{\boldsymbol{\psi_j} \,|\, j = 1, \dots, N_H\}$ is a basis of H_h^d while $\{\chi_j \,|\, j = 1, \dots, N_L\}$ is a basis of L_h. This especially means

$$\boldsymbol{M x^k} + k\boldsymbol{A x^k} + k\boldsymbol{B y^k} = \boldsymbol{b^k}. \tag{4.9}$$

Since $\boldsymbol{v_h^k}$ converges point-wise to $\boldsymbol{v_h^0}$, we have $\boldsymbol{x^k} \to \boldsymbol{x^0}$ with

$$\boldsymbol{v_h^0} = \sum_{j=1}^{N_H} x_j^0 \boldsymbol{\psi_j}.$$

For $k \to 0$, we have

$$\boldsymbol{b^k} \to \boldsymbol{b^0} = \big((\boldsymbol{v_H}, \boldsymbol{\psi_i})\big)_{i=1,\dots,N_H} = \boldsymbol{M}\bar{\boldsymbol{x}},$$

because $\boldsymbol{v_H}$ and $\boldsymbol{f}$ do not depend on time, and $\bar{\boldsymbol{x}} \in \mathbb{R}^{N_H}$ is given by

$$\boldsymbol{P_h v_H} = \sum_{j=1}^{N_H} \bar{x}_j \boldsymbol{\psi_j}.$$

In virtue of (4.9), we conclude that $k\boldsymbol{y^k}$ converges for $k \to 0$, too. We denote the limit by $\boldsymbol{y^0}$. Hence, by passing to the limit $k \to 0$ in (4.9), we obtain

$$\boldsymbol{M x^0} + \boldsymbol{B y^0} = \boldsymbol{M}\bar{\boldsymbol{x}}. \tag{4.10}$$

Then by defining

$$p_h^0 = \sum_{j=1}^{N_L} y_j^0 \chi_j \in L_h,$$

equation (4.10) may equivalently be written as

$$(\boldsymbol{v_h^0}, \boldsymbol{\psi}) - (p_h^0, \nabla \cdot \boldsymbol{\psi}) = (\boldsymbol{P_h v_H}, \boldsymbol{\psi}) = (\boldsymbol{v_H}, \boldsymbol{\psi}) \quad \forall \boldsymbol{\psi} \in H_h^d,$$

which together with the second equation in (4.8) states that $\boldsymbol{v_h^0}$ is just the H-projection of $\boldsymbol{v_H}$ into H_h^d. In particular $\boldsymbol{v_h^0}$ is uniquely determined and convergence in Lemma 4.1 is obtained for any sequence $k \to 0$.

To continue, we note that if $\boldsymbol{y^0} = \boldsymbol{0}$ we have $\boldsymbol{x^0} = \bar{\boldsymbol{x}}$ or equivalently $\boldsymbol{P_h v_H} = \boldsymbol{v_h^0} = \widetilde{\boldsymbol{P}}_{\boldsymbol{h}} \boldsymbol{v_H}$. Otherwise $\boldsymbol{y^0} \neq \boldsymbol{0}$, hence there is $j \in \{\, 1, \dots, N_L \,\}$ with $y_j^0 \neq 0$ and thus by definition $ky_j^k \not\to 0$. This means there exists some constant $C(h) > 0$ such that

$$|y_j^k| \geq C(h) k^{-1} \quad \text{and hence} \quad \|p_h^k\| \geq C(h) k^{-1}.$$

□

Remark 4.3. *If $\mathcal{T}_h$ is obtained from $\mathcal{T}_H$ by uniform refinement, then we obviously have $H_H \subseteq H_h$ as well as $L_H \subseteq L_h$ and thus the L^2-projection from H_H onto H_h is the identity mapping. As a consequence, we have $\boldsymbol{P_h v_H} = \boldsymbol{v_H}$. However, in general, we have*

$$(\nabla \cdot \boldsymbol{v_H}, \chi) \neq 0$$

for $\chi \in L_h \setminus L_H$ also in this case and hence $\boldsymbol{P_h v_H} \neq \widetilde{\boldsymbol{P}}_{\boldsymbol{h}} \boldsymbol{v_H}$.

In the remaining part of this section, we want to show that the pressure approximations $\hat{p}_h^k$ obtained through equation (4.5) remain bounded for $k \to 0$.

To do so, we introduce some auxiliary quantities: Similar to (4.3), let the approximate solution $(\boldsymbol{v_h}, p_h)^T \in H_h^d \times L_h$ of the Stokes problem on the mesh $\mathcal{T}_h$ be given by

$$\begin{aligned} (\nabla \boldsymbol{v_h}, \nabla \boldsymbol{\psi}) - (p_h, \nabla \cdot \boldsymbol{\psi}) &= (\boldsymbol{f}, \boldsymbol{\psi}) \qquad && \forall \boldsymbol{\psi} \in H_h^d, \\ (\nabla \cdot \boldsymbol{v_h}, \chi) &= 0 && \forall \chi \in L_h. \end{aligned} \tag{4.11}$$

Then, in addition to the H-projection $\widetilde{\boldsymbol{P}}_{\boldsymbol{h}} \boldsymbol{v}$ of the continuous velocity $\boldsymbol{v}$ defined by (4.6), we consider the V-projection $\widetilde{\boldsymbol{R}}_{\boldsymbol{h}} \boldsymbol{v}$ of the continuous velocity $\boldsymbol{v}$ into H_h^d. It is given as the first component of the solution $(\widetilde{\boldsymbol{R}}_{\boldsymbol{h}} \boldsymbol{v}, \tilde{r}_h)^T \in H_h^d \times L_h$ of

$$\begin{aligned} (\nabla \widetilde{\boldsymbol{R}}_{\boldsymbol{h}} \boldsymbol{v}, \nabla \boldsymbol{\psi}) - (\tilde{r}_h, \nabla \cdot \boldsymbol{\psi}) &= (\nabla \boldsymbol{v}, \nabla \boldsymbol{\psi}) \qquad && \forall \boldsymbol{\psi} \in H_h^d, \\ (\nabla \cdot \widetilde{\boldsymbol{R}}_{\boldsymbol{h}} \boldsymbol{v}, \chi) &= 0 && \forall \chi \in L_h. \end{aligned} \tag{4.12}$$

Again, it is clear that for any $\boldsymbol{v} \in H_0^1(\Omega)^d$ it holds $\|\nabla \widetilde{\boldsymbol{R}}_{\boldsymbol{h}} \boldsymbol{v}\| \leq \|\nabla \boldsymbol{v}\|$.

Lemma 4.4. *The pressure $\hat{p}_h^k$ given by (4.5) is bounded independent of k.*

Proof. Subtracting k^{-1} times the first equation of (4.6) from the first equation of (4.4) leads to

$$k^{-1}(\boldsymbol{v_h^k} - \widetilde{\boldsymbol{P}}_{\boldsymbol{h}} \boldsymbol{v_H}, \boldsymbol{\psi}) + (\nabla \boldsymbol{v_h^k}, \nabla \boldsymbol{\psi}) - k^{-1}(k p_h^k - \tilde{p}_h^H, \nabla \cdot \boldsymbol{\psi}) = (\boldsymbol{f}, \boldsymbol{\psi}) \quad \forall \boldsymbol{\psi} \in H_h^d$$

or equivalently

$$\begin{aligned} k^{-1}(\boldsymbol{v_h^k} - \widetilde{\boldsymbol{P}}_{\boldsymbol{h}} \boldsymbol{v_H}, \boldsymbol{\psi}) + (\nabla(\boldsymbol{v_h^k} - \widetilde{\boldsymbol{P}}_{\boldsymbol{h}} \boldsymbol{v_H}), \nabla \boldsymbol{\psi}) - k^{-1}(k p_h^k - \tilde{p}_h^H, \nabla \cdot \boldsymbol{\psi}) \\ = (\boldsymbol{f}, \boldsymbol{\psi}) - (\nabla \widetilde{\boldsymbol{P}}_{\boldsymbol{h}} \boldsymbol{v_H}, \nabla \boldsymbol{\psi}) \quad \forall \boldsymbol{\psi} \in H_h^d. \end{aligned}$$

By testing with $\boldsymbol{\psi} = \boldsymbol{v_h^k} - \widetilde{\boldsymbol{P}}_{\boldsymbol{h}} \boldsymbol{v_H} \in H_h^d$, we obtain

$$\begin{aligned} k^{-1}\|\boldsymbol{v_h^k} - \widetilde{\boldsymbol{P}}_{\boldsymbol{h}} \boldsymbol{v_H}\|^2 + \|\nabla(\boldsymbol{v_h^k} - \widetilde{\boldsymbol{P}}_{\boldsymbol{h}} \boldsymbol{v_H})\|^2 \\ = (\boldsymbol{f}, \boldsymbol{v_h^k} - \widetilde{\boldsymbol{P}}_{\boldsymbol{h}} \boldsymbol{v_H}) - (\nabla \widetilde{\boldsymbol{P}}_{\boldsymbol{h}} \boldsymbol{v_H}, \nabla(\boldsymbol{v_h^k} - \widetilde{\boldsymbol{P}}_{\boldsymbol{h}} \boldsymbol{v_H})), \end{aligned} \tag{4.13}$$

because the other terms cancel out due to the second equations of (4.4) and (4.6). We then have for arbitrary $\boldsymbol{\psi} \in H_h^d$

$$\begin{aligned} |(\nabla \widetilde{\boldsymbol{P}}_{\boldsymbol{h}} \boldsymbol{v_H}, \nabla \boldsymbol{\psi})| &= |(\nabla(\widetilde{\boldsymbol{P}}_{\boldsymbol{h}} \boldsymbol{v_H} - \widetilde{\boldsymbol{R}}_{\boldsymbol{h}} \boldsymbol{v}), \nabla \boldsymbol{\psi}) + (\nabla(\widetilde{\boldsymbol{R}}_{\boldsymbol{h}} \boldsymbol{v} - \boldsymbol{v}), \nabla \boldsymbol{\psi}) + (\nabla \boldsymbol{v}, \nabla \boldsymbol{\psi})| \\ &\leq \big\{\|\nabla(\widetilde{\boldsymbol{P}}_{\boldsymbol{h}} \boldsymbol{v_H} - \widetilde{\boldsymbol{R}}_{\boldsymbol{h}} \boldsymbol{v})\| + \|\nabla(\widetilde{\boldsymbol{R}}_{\boldsymbol{h}} \boldsymbol{v} - \boldsymbol{v})\|\big\}\|\nabla \boldsymbol{\psi}\| + |(\Delta \boldsymbol{v}, \boldsymbol{\psi})| \\ &\leq C\big\{h^{-2}\|\widetilde{\boldsymbol{P}}_{\boldsymbol{h}} \boldsymbol{v_H} - \widetilde{\boldsymbol{R}}_{\boldsymbol{h}} \boldsymbol{v}\| + h^{-1}\|\nabla(\widetilde{\boldsymbol{R}}_{\boldsymbol{h}} \boldsymbol{v} - \boldsymbol{v})\| + \|\Delta \boldsymbol{v}\|\big\}\|\boldsymbol{\psi}\| \\ &\leq Ch^{-2}\big\{\|\widetilde{\boldsymbol{P}}_{\boldsymbol{h}} \boldsymbol{v_H} - \widetilde{\boldsymbol{P}}_{\boldsymbol{h}} \boldsymbol{v}\| + \|\widetilde{\boldsymbol{P}}_{\boldsymbol{h}} \boldsymbol{v} - \boldsymbol{v}\| + \|\boldsymbol{v} - \widetilde{\boldsymbol{R}}_{\boldsymbol{h}} \boldsymbol{v}\| \\ &\qquad + h\|\nabla(\widetilde{\boldsymbol{R}}_{\boldsymbol{h}} \boldsymbol{v} - \boldsymbol{v})\| + h^2\|\Delta \boldsymbol{v}\|\big\}\|\boldsymbol{\psi}\|, \end{aligned} \tag{4.14}$$

where in the penultimate line inverse estimates have been used. We will now treat each term on the right-hand side of (4.14) separately.

By continuity of the H-projection and standard approximation results (see, for instance, [11]) and the a priori estimate (4.2), we obtain

$$\|\widetilde{\boldsymbol{P}}_{\boldsymbol{h}}\boldsymbol{v}_{\boldsymbol{H}} - \widetilde{\boldsymbol{P}}_{\boldsymbol{h}}\boldsymbol{v}\| \leq \|\boldsymbol{v} - \boldsymbol{v}_{\boldsymbol{H}}\| \leq CH^2\big\{\|\boldsymbol{v}\|_{H^2} + \|p\|_{H^1}\big\} \leq CH^2\|\boldsymbol{f}\|. \tag{4.15}$$

In order to estimate the next term, we note that by best-approximation of the H-projection

$$\|\widetilde{\boldsymbol{P}}_{\boldsymbol{h}}\boldsymbol{v} - \boldsymbol{v}\| \leq \|\boldsymbol{v} - \boldsymbol{v}_{\boldsymbol{h}}\| \leq Ch^2\|\boldsymbol{f}\|. \tag{4.16}$$

From best-approximation of the V-projection we get

$$\|\nabla(\widetilde{\boldsymbol{R}}_{\boldsymbol{h}}\boldsymbol{v} - \boldsymbol{v})\| \leq \|\nabla(\boldsymbol{v} - \boldsymbol{v}_{\boldsymbol{h}})\| \leq Ch\|\boldsymbol{f}\|. \tag{4.17}$$

Using standard error estimates for the V-projection, see, e. g. [20], yields

$$\|\boldsymbol{v} - \widetilde{\boldsymbol{R}}_{\boldsymbol{h}}\boldsymbol{v}\| \leq Ch^2\|\boldsymbol{f}\|. \tag{4.18}$$

Finally, we obviously have

$$\|\Delta\boldsymbol{v}\| \leq \|\boldsymbol{v}\|_{H^2} \leq C\|\boldsymbol{f}\|. \tag{4.19}$$

Inserting the estimates (4.15), (4.16), (4.17), (4.18), and (4.19) into (4.14) then yields

$$|(\nabla\widetilde{\boldsymbol{P}}_{\boldsymbol{h}}\boldsymbol{v}_{\boldsymbol{H}}, \nabla\boldsymbol{\psi})| \leq C\big(1 + (\tfrac{H}{h})^2\big)\|\boldsymbol{f}\|\|\boldsymbol{\psi}\|.$$

Since we only consider uniform refinement or uniform coarsening, we have $H = 2h$ or $H = \frac{1}{2}h$ and thus

$$|(\nabla\widetilde{\boldsymbol{P}}_{\boldsymbol{h}}\boldsymbol{v}_{\boldsymbol{H}}, \nabla\boldsymbol{\psi})| \leq C\|\boldsymbol{f}\|\|\boldsymbol{\psi}\|. \tag{4.20}$$

This allows us to conclude from (4.13):

$$\begin{aligned} k^{-1}\|\boldsymbol{v}_{\boldsymbol{h}}^{\boldsymbol{k}} - \widetilde{\boldsymbol{P}}_{\boldsymbol{h}}\boldsymbol{v}_{\boldsymbol{H}}\|^2 + \|\nabla(\boldsymbol{v}_{\boldsymbol{h}}^{\boldsymbol{k}} - \widetilde{\boldsymbol{P}}_{\boldsymbol{h}}\boldsymbol{v}_{\boldsymbol{H}})\|^2 &\leq \|\boldsymbol{f}\|\|\boldsymbol{v}_{\boldsymbol{h}}^{\boldsymbol{k}} - \widetilde{\boldsymbol{P}}_{\boldsymbol{h}}\boldsymbol{v}_{\boldsymbol{H}}\| + |(\nabla\widetilde{\boldsymbol{P}}_{\boldsymbol{h}}\boldsymbol{v}_{\boldsymbol{H}}, \nabla(\boldsymbol{v}_{\boldsymbol{h}}^{\boldsymbol{k}} - \widetilde{\boldsymbol{P}}_{\boldsymbol{h}}\boldsymbol{v}_{\boldsymbol{H}}))| \\ &\leq C\|\boldsymbol{f}\|\|\boldsymbol{v}_{\boldsymbol{h}}^{\boldsymbol{k}} - \widetilde{\boldsymbol{P}}_{\boldsymbol{h}}\boldsymbol{v}_{\boldsymbol{H}}\| \end{aligned}$$

and hence

$$k^{-1}\|\boldsymbol{v}_{\boldsymbol{h}}^{\boldsymbol{k}} - \widetilde{\boldsymbol{P}}_{\boldsymbol{h}}\boldsymbol{v}_{\boldsymbol{H}}\| \leq C\|\boldsymbol{f}\|. \tag{4.21}$$

By using the Poincaré inequality, we also obtain from (4.20)

$$|(\nabla\widetilde{\boldsymbol{P}}_{\boldsymbol{h}}\boldsymbol{v}_{\boldsymbol{H}}, \nabla\boldsymbol{\psi})| \leq C\|\boldsymbol{f}\|\|\nabla\boldsymbol{\psi}\| \tag{4.22}$$

and therefore from (4.13) also

$$\|\nabla(\boldsymbol{v}_{\boldsymbol{h}}^{\boldsymbol{k}} - \widetilde{\boldsymbol{P}}_{\boldsymbol{h}}\boldsymbol{v}_{\boldsymbol{H}})\| \leq C\|\boldsymbol{f}\|. \tag{4.23}$$

To show that $\|\hat{p}_h^k\|$ remains bounded for $k \to 0$, we use the inf-sup condition (2.2) and the fact that $\boldsymbol{v}_{\boldsymbol{h}}^{\boldsymbol{k}} = \hat{\boldsymbol{v}}_{\boldsymbol{h}}^{\boldsymbol{k}}$ which allows us to replace $\hat{\boldsymbol{v}}_{\boldsymbol{h}}^{\boldsymbol{k}}$ by $\boldsymbol{v}_{\boldsymbol{h}}^{\boldsymbol{k}}$ in (4.5) to obtain:

$$\begin{aligned} \beta\|\hat{p}_h^k\| &\leq \sup_{\boldsymbol{\psi}\in H_h^d} \frac{(\hat{p}_h^k, \nabla\cdot\boldsymbol{\psi})}{\|\nabla\boldsymbol{\psi}\|} \\ &= \sup_{\boldsymbol{\psi}\in H_h^d} \frac{k^{-1}(\boldsymbol{v}_{\boldsymbol{h}}^{\boldsymbol{k}} - \widetilde{\boldsymbol{P}}_{\boldsymbol{h}}\boldsymbol{v}_{\boldsymbol{H}}, \boldsymbol{\psi}) + (\nabla(\boldsymbol{v}_{\boldsymbol{h}}^{\boldsymbol{k}} - \widetilde{\boldsymbol{P}}_{\boldsymbol{h}}\boldsymbol{v}_{\boldsymbol{H}}), \nabla\boldsymbol{\psi}) + (\nabla\widetilde{\boldsymbol{P}}_{\boldsymbol{h}}\boldsymbol{v}_{\boldsymbol{H}}, \nabla\boldsymbol{\psi}) - (\boldsymbol{f}, \boldsymbol{\psi})}{\|\nabla\boldsymbol{\psi}\|} \\ &\leq Ck^{-1}\|\boldsymbol{v}_{\boldsymbol{h}}^{\boldsymbol{k}} - \widetilde{\boldsymbol{P}}_{\boldsymbol{h}}\boldsymbol{v}_{\boldsymbol{H}}\| + \|\nabla(\boldsymbol{v}_{\boldsymbol{h}}^{\boldsymbol{k}} - \widetilde{\boldsymbol{P}}_{\boldsymbol{h}}\boldsymbol{v}_{\boldsymbol{H}})\| + \sup_{\boldsymbol{\psi}\in H_h^d} \frac{|(\nabla\widetilde{\boldsymbol{P}}_{\boldsymbol{h}}\boldsymbol{v}_{\boldsymbol{H}}, \nabla\boldsymbol{\psi})|}{\|\nabla\boldsymbol{\psi}\|} + C\|\boldsymbol{f}\| \\ &\leq C\|\boldsymbol{f}\|. \end{aligned}$$

Here, the estimates (4.21), (4.22), and (4.23) have been used. Since the right-hand side is independent of k, we have shown that $\|\hat{p}_h^k\|$ remains bounded for $k \to 0$. □

Remark 4.5. *The arguments used above to show that* $\|p_h^k\| \geq C(h)k^{-1}$ *if there is a* $\chi \in L_h$ *such that* $(\nabla \cdot \boldsymbol{P_h v_H}, \chi) \neq 0$ *are not restricted to the case of uniform refinement or coarsening of the meshes. Actually, they directly carry over to the case of arbitrary refinement or coarsening of cells. The estimate for the boundedness of* $\|\hat{p}_h^k\|$ *can be generalized as long as we are able to bound* $\|\nabla \widetilde{\boldsymbol{P}}_{\boldsymbol{h}} \boldsymbol{v_H}\|$ *and* $\|\tilde{\Delta}_h \widetilde{\boldsymbol{P}}_{\boldsymbol{h}} \boldsymbol{v_H}\|$ *where* $\tilde{\Delta}_h \widetilde{\boldsymbol{P}}_{\boldsymbol{h}} \boldsymbol{v_H}$ *denotes the discrete Stokes operator of* $\widetilde{\boldsymbol{P}}_{\boldsymbol{h}} \boldsymbol{v_H}$ *given by*

$$(\tilde{\Delta}_h \widetilde{\boldsymbol{P}}_{\boldsymbol{h}} \boldsymbol{v_H}, \boldsymbol{\psi}) = -(\nabla \widetilde{\boldsymbol{P}}_{\boldsymbol{h}} \boldsymbol{v_H}, \nabla \boldsymbol{\psi}) \quad \forall \boldsymbol{\psi} \in H_h^d \cap \left\{ \boldsymbol{\psi} \;\middle|\; (\nabla \cdot \boldsymbol{\psi}, \chi) = 0 \ \forall \chi \in L_h \right\}.$$

We showed that on dynamic spatial meshes bounded pressure approximations are only possible if the L^2-projection of the velocity from the first mesh is divergence-free with respect to the test functions of the new mesh. Otherwise, the pressure approximation contains k^{-1} times the Lagrange multiplier occurring in the H-projection of the old velocity field into the new finite element space which leads to the unbounded behavior for $k \to 0$.

5. SOLUTION OF THE PROBLEM

The following Subsection 5.1 presents some attempts to solve the problem discussed in this article.

5.1. Attempts to solve this problem

We have seen in the previous section that the error in the pressure occurring when switching the spatial mesh decreases with (at least) the same order as the spatial discretization error for $h \to 0$, but increases like $O(k^{-1})$ for $k \to 0$. We showed that this effect does not originate from the stabilization since the inf-sup-stable Taylor-Hood element also produces qualitatively the same error. In this subsection, we discuss some attempts to overcome this problem and obtain pressure approximations which remain bounded for $k \to 0$.

We also showed analytically that the error in the pressure approximation which is solely located in the first time step on a new spatial mesh is unavoidable if the L^2-projection of the old velocity field is not divergence-free with respect to test functions of the new finite element space for the pressure. However, the proposed approach to solving this problem namely taking the divergence-free L^2-projection as initial values on the new spatial mesh might be too costly to perform each time the mesh is changed. Therefore, we present two alternatives to the H-projection that might be easier to implement or less costly. We remark that differences are gradually as in principal all proposed methods can be solved in linear time with respect to the degrees of freedom provided sufficient effort has been spent on the implementation of a suitable solver. However, as we will see in Section 5.2 both alternatives introduce additional errors that may accumulate under frequent mesh changes.

To sum up, the three "ideas" discussed in this section are:

Divergence-free $\boldsymbol{L^2}$-projection ($\boldsymbol{H}$-projection):
After computing $(\boldsymbol{V_{m-1}}, P_{m-1})^T \in (H_h^{m-1})^d \times L_h^{m-1}$ first compute a projection $\widetilde{\boldsymbol{V}}_{\boldsymbol{m-1}}$

of $\boldsymbol{V_{m-1}}$ into $(H_h^m)^d$ which is divergence-free with respect to test functions in $(H_h^m)^d$ and use this projection as initial values for the next time step. The projection is determined by

$$\begin{aligned}(\widetilde{\boldsymbol{V}}_{\boldsymbol{m-1}}, \boldsymbol{\psi}) - (\widetilde{P}, \nabla \cdot \boldsymbol{\psi}) &= (\boldsymbol{V_{m-1}}, \boldsymbol{\psi}) \qquad && \forall \boldsymbol{\psi} \in (H_h^m)^d, \\ (\nabla \cdot \widetilde{\boldsymbol{V}}_{\boldsymbol{m-1}}, \chi) &= 0 && \forall \chi \in L_h^m.\end{aligned} \tag{5.1}$$

As we have shown in Section 4.2 this projection removes the undesired $O(k^{-1})$ error in the pressure. Unfortunately, the efficient solution of (5.1) requires different solvers than the efficient solution of a time step. This means that additional effort has to be spent on the implementation.

Divergence-free $\boldsymbol{H_0^1}$-projection ($\boldsymbol{V}$-projection):
Same procedure as for "Divergence-free L^2-projection", but this time the projection is determined by

$$\begin{aligned}(\nabla\widetilde{\boldsymbol{V}}_{\boldsymbol{m-1}}, \nabla\boldsymbol{\psi}) - (\widetilde{P}, \nabla \cdot \boldsymbol{\psi}) &= (\nabla\boldsymbol{V_{m-1}}, \nabla\boldsymbol{\psi}) \qquad && \forall \boldsymbol{\psi} \in (H_h^m)^d, \\ (\nabla \cdot \widetilde{\boldsymbol{V}}_{\boldsymbol{m-1}}, \chi) &= 0 && \forall \chi \in L_h^m.\end{aligned} \tag{5.2}$$

In contrast to (5.1) the solution of (5.2) can be done by the same solver routines required for the solution of a newton step of the nonlinear problem. However, it requires that matrices are specially assembled.

Repeating one time step:
After computing $(\boldsymbol{V_{m-1}}, P_{m-1})^T \in (H_h^{m-1})^d \times L_h^{m-1}$ repeat the current time step to determine approximations $(\widetilde{\boldsymbol{V}}_{\boldsymbol{m-1}}, \widetilde{P}_{m-1})^T \in (H_h^m)^d \times L_h^m$ for $t = t_{m-1}$, but already in the finite element spaces corresponding to $t = t_m$. One can hope that then only $\widetilde{P}_{m-1}$ contains this error and since $\widetilde{\boldsymbol{V}}_{\boldsymbol{m-1}}$ is divergence-free with respect to test functions in L_h^m this error does not occur again when computing $(\boldsymbol{V_m}, P_m)^T \in (H_h^m)^d \times L_h^m$ using the initial values $\widetilde{\boldsymbol{V}}_{\boldsymbol{m-1}}$.

As for the V-projection (5.2) the solution of this problem can be done using the same solver routines required for the solution of a newton step of the nonlinear problem. In contrast to the solution of (5.2) it is possible to reuse the matrices built for the computation of the time step. Hence it is potentially faster than (5.2). Unfortunately the problem is nonlinear, and hence possibly several linear system solves are required making the advantage over (5.2) less obvious.

For the equal-order spatial discretizations $\mathcal{Q}_1/\mathcal{Q}_1$ and $\mathcal{Q}_2/\mathcal{Q}_2$ the variational formulations given above have to be stabilized, of course. This is once again done by means of the local projection stabilization.

Since the behavior of the pressure error is already of the right order for $h \to 0$, we discuss in this subsection only the influence of the presented "ideas" on the development of the error under uniform temporal refinement. We repeat the investigation of Section 4.1.2 using the proposed modifications.

5.1.1. H-projection In this subsection, we present the development of the pressure error when using the H-projection of the old velocity field into the new finite element space as initial values when switching the spatial mesh.

Table III: Convergence order of $\|\overline{p} - p_{kh}\|$ under temporal refinement with fixed spatial mesh size $h = \frac{1}{16}$ with different spatial and temporal discretizations at the mesh directly following the change of the spatial meshes using H-projection

	dG(0)		dG(1)		fractional-step-θ	
	$t = 3 + k$	$t = 6 + k$	$t = 3 + k$	$t = 6 + k$	$t = 3 + k$	$t = 6 + k$
$\mathcal{Q}_1/\mathcal{Q}_1$	−0.04	0.00	−0.03	0.00	−0.06	0.00
$\mathcal{Q}_2/\mathcal{Q}_2$	0.00	−0.14	0.06	−0.17	0.07	−0.15
$\mathcal{Q}_2/\mathcal{Q}_1$	−0.15	−0.07	−0.16	−0.08	−0.13	−0.08

Table IV: Convergence order of $\|\overline{p} - p_{kh}\|$ under temporal refinement with fixed spatial mesh size $h = \frac{1}{16}$ with different spatial and temporal discretizations at the mesh directly following the change of the spatial meshes using V-projection

	dG(0)		dG(1)		fractional-step-θ	
	$t = 3 + k$	$t = 6 + k$	$t = 3 + k$	$t = 6 + k$	$t = 3 + k$	$t = 6 + k$
$\mathcal{Q}_1/\mathcal{Q}_1$	−0.20	0.00	−0.26	0.00	−0.20	0.00
$\mathcal{Q}_2/\mathcal{Q}_2$	−0.14	−0.01	−0.16	−0.01	−0.13	−0.01
$\mathcal{Q}_2/\mathcal{Q}_1$	−0.14	0.00	−0.15	−0.01	−0.12	0.00

The results under uniform temporal refinement are listed in Tables III for the $\mathcal{Q}_1/\mathcal{Q}_1$, $\mathcal{Q}_2/\mathcal{Q}_2$ and $\mathcal{Q}_2/\mathcal{Q}_1$ spatial discretization, respectively.

We can conclude that using the H-projection of the velocity of the last time step into the new finite element space as initial values leads to pressure errors which are bounded for $k \to 0$ as predicted by our analysis in Section 4.2. Actually, the pressure error becomes almost independent of k.

5.1.2. V-projection In this subsection, we present the development of the pressure error when using the V-projection of the old velocity field into the new finite element space as initial values when switching the spatial mesh.

The results under uniform temporal refinement are listed in Tables IV for the $\mathcal{Q}_1/\mathcal{Q}_1$, $\mathcal{Q}_2/\mathcal{Q}_2$, and $\mathcal{Q}_2/\mathcal{Q}_1$ spatial discretization, respectively.

Using the V-projection of the old velocity into the new finite element space also leads to pressure errors which remain bounded for $k \to 0$.

5.1.3. Repeating one time step In this subsection, we present the development of the pressure error when repeating the last time step of the old spatial mesh on the new one to determine the initial values for the first real time step on the new mesh.

The results under uniform temporal refinement are listed in Tables V for the $\mathcal{Q}_1/\mathcal{Q}_1$, $\mathcal{Q}_2/\mathcal{Q}_2$, and $\mathcal{Q}_2/\mathcal{Q}_1$ spatial discretization, respectively.

We observe for all spatial discretizations that repeating one time step leads to a slower increase of the error in the pressure when switching the spatial mesh from $\mathcal{T}_{2h}$ to $\mathcal{T}_h$ and to an almost constant error when switching from $\mathcal{T}_h$ to $\mathcal{T}_{2h}$.

Table V: Convergence order of $\|\overline{p} - p_{kh}\|$ under temporal refinement with fixed spatial mesh size $h = \frac{1}{16}$ with different spatial and temporal discretizations at the mesh directly following the change of the spatial meshes with repetition of one time step

	dG(0)		dG(1)		fractional-step-θ	
	$t = 3 + k$	$t = 6 + k$	$t = 3 + k$	$t = 6 + k$	$t = 3 + k$	$t = 6 + k$
$\mathcal{Q}_1/\mathcal{Q}_1$	−0.46	0.00	−0.61	0.00	−0.43	0.00
$\mathcal{Q}_2/\mathcal{Q}_2$	−0.31	0.01	−0.37	0.02	−0.34	−0.10
$\mathcal{Q}_2/\mathcal{Q}_1$	−0.31	−0.13	−0.37	−0.14	−0.20	−0.09

Remark 5.1. *We remark that the behavior of the fractional-step-θ scheme is hardly a surprise given the results from Section 4.1.2. However, after our analysis in Section 4.2 we can now explain, why the fractional-step-θ scheme doesn't show the undesired divergence of the pressure even without modifications. Namely we saw that the divergence of the pressure is localized to the first time step after changing the mesh. However, in the fractional-step-θ scheme this is only the first substep of a complete time step. Hence, one ignores this "solution" as it is only an intermediate quantity. This gives rise to another method to overcome this defect. Namely, one may neglect the time step immediately after changing the spatial mesh.*

5.2. Application to the benchmark problem

We have seen that all three "ideas" are able to (almost) remove the $O(k^{-1})$ increase in the pressure error while the H-projection performed best.

In this subsection, in order to compare all strategies, we return to the benchmark configuration "Laminar Flow Around a Cylinder" with constant inflow and Reynolds number $\mathrm{Re} = 20$ which possesses a stationary solution. The discretization used here is again the dG(0) method in time with a $\mathcal{Q}_1/\mathcal{Q}_1$ discretization in space involving local projection stabilization. In Figure 8, the temporal evolution of the lift-coefficient is depicted for different choices of the initial value. For completeness, we also show the results of the fractional-step-θ scheme combined with a $\mathcal{Q}_1/\mathcal{Q}_1$ discretization in space and local projection stabilization. The upper picture shows the development when switching the spatial mesh from $\mathcal{T}_{2h}$ to $\mathcal{T}_h$ which corresponds to a uniform refinement, while the lower picture shows the lift-coefficient when switching from $\mathcal{T}_h$ to $\mathcal{T}_{2h}$ which corresponds to a uniform coarsening. The labeling of the different curves is as follows:

- "original": No additional operations are performed when switching the spatial mesh.
- "H-projection": When switching the spatial mesh, the H-projection of the old velocity into the new finite element space is used as initial values for the new time step.
- "V-projection": When switching the spatial mesh, the V-projection of the old velocity into the new finite element space is used as initial values for the new time step.
- "repeat": When switching the spatial mesh, the last time step is repeated already on the new mesh to obtain initial values.

When looking at the upper picture of Figure 8, we note the large error in the lift-coefficient for the "original" method. The curves of the "H-projection" and "V-projection" show a slightly different temporal evolution where the "H-projection" approaches the "original" curve faster.

Repeating one time step leads to a temporal evolution of the lift-coefficient which is close to the values produced by the fractional-step-θ scheme.

If we consider the lower picture of Figure 8 which shows the temporal evolution of the lift-coefficient under a uniform coarsening of the spatial mesh, we observe quite large differences between the different strategies. While the "H-projection" mainly eliminates the large error of the "original" curve and stays very close to it elsewhere. The other "ideas" lead to completely different temporal evolutions of the lift-coefficient. Of course, for $t \to \infty$, those values converge to the same stationary limit as the other methods. The fractional-step-θ scheme mainly leads to the same evolution of the lift-coefficient as the "H-projection".

In computations the choice of either of these methods might be advantageous over the others depending on which of the problems can be solved more efficiently by a given flow solver. However, we see from Figure 8 that both V-projection and repetition of a time step give rise to significantly larger errors, especially when coarsening of the mesh occurs. However even the H-projection is not optimal when refining the mesh. This leads to the conclusion that the apparently best possibility lies in neglecting the time step directly after the spatial mesh changes, possibly by adding an intermediate time step as it is done in the fractional-step-θ scheme.

To conclude this subsection, let us reconsider the initial time-dependent benchmark problem from Section 3.1. Figure 9 shows the temporal evolution of the lift-coefficient after five iterations of adaptive temporal and spatial refinement using dynamic meshes in combination with the H-projection (left picture) or the V-projection (right picture) each time the spatial mesh is changed. We observe that the oscillations showing up without using additional projection steps when changing the spatial mesh (see Figure 3) have vanished. Furthermore, we note a slightly different temporal evolution of the lift-coefficient, especially at the end of the time interval. This is due to the fact that the adaptive refinement leads to different meshes and time step sizes when applying projection steps. However, the temporal evolution depicted in Figure 9 is closer to that of the reference solution, see [28].

CONCLUSIONS

In this article we analyzed the behavior of the pressure on changing spatial meshes during the computation of nonstationary incompressible fluid flows for several time stepping schemes. In particular, we showed that whenever the spatial mesh is changed between two time steps the discrete pressure will in general diverge with order k^{-1} in the following time step. This behavior was proven, for the dG(0) time discretization, to be due to the fact that discrete solenoidal vector fields lose this property under changes of the discrete spaces. Finally we showed that this defect can be removed by an appropriate projection step. However, as the defect is localized in time, the most promising alternative, from a computational point of view, is to add an additional intermediate time step that is neglected when evaluating the pressure.

ACKNOWLEDGEMENTS

The authors would like to thank Rolf Rannacher for his valuable comments on this manuscript.

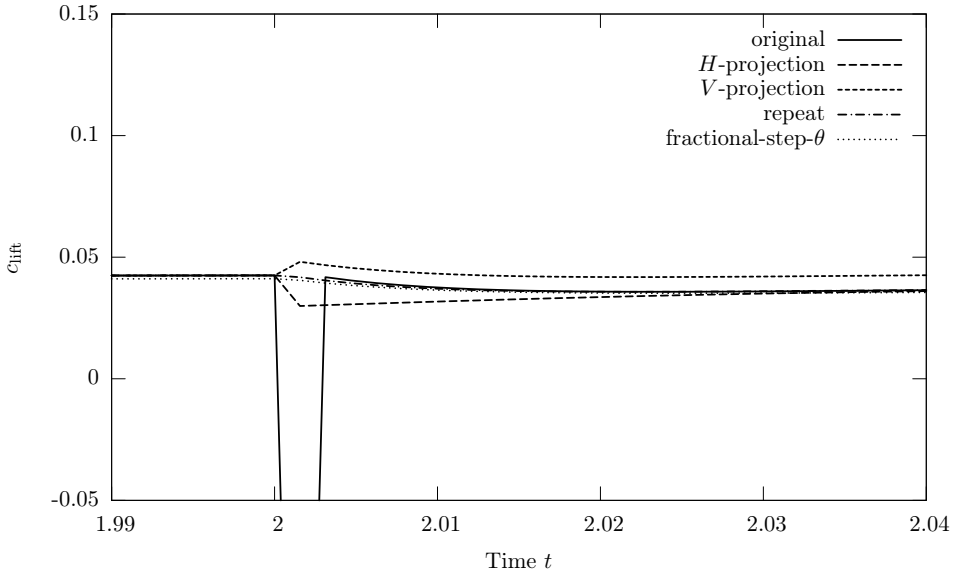

(a) Switching from $\mathcal{T}_{2h}$ to $\mathcal{T}_h$

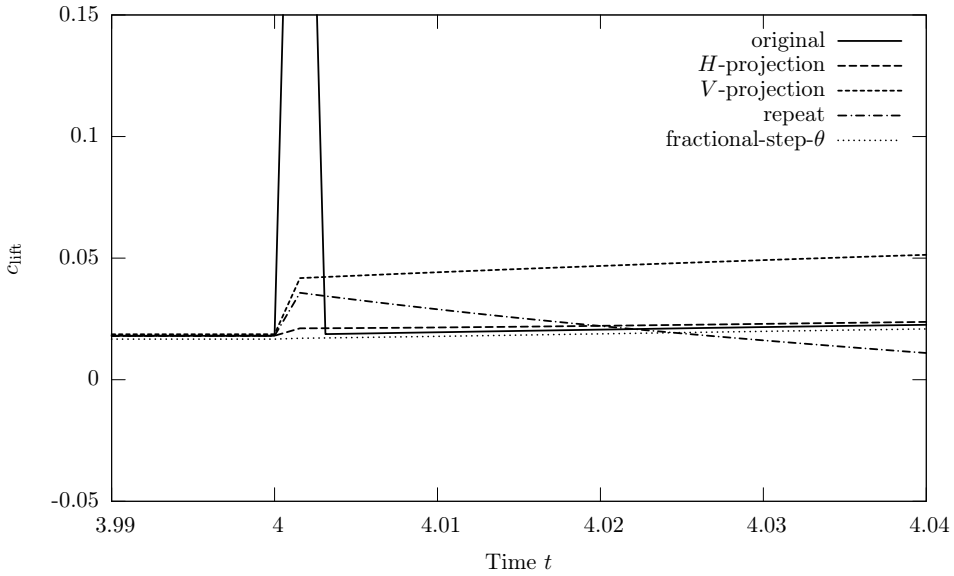

(b) Switching from $\mathcal{T}_h$ to $\mathcal{T}_{2h}$

Figure 8: Temporal evolution of the lift-coefficient for different initial values

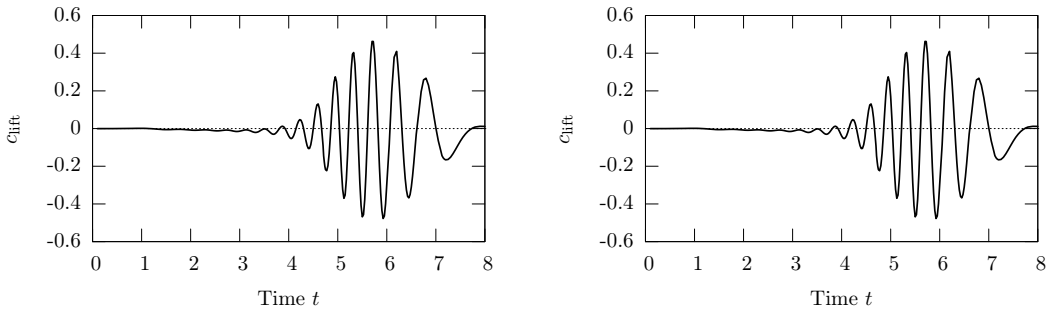

(a) H-projection (b) V-projection

Figure 9: Lift-coefficient c_{lift} after five adaptation cycles with different types of projection steps

REFERENCES

1. Schäfer M, Turek S. Benchmark computations of laminar flow around a cylinder. *Flow Simulation with High-Performance Computer II*, *Notes on Numerical Fluid Mechanics*, vol. 52, Hirschel EH (ed.), Vieweg: Braunschweig Wiesbaden, 1996; 547–566.
2. Verfürth R. *A Review of A Posteriori Error Estimation and Adaptive Mesh-Refinement Techniques*. Wiley-Teubner Series Advances in Numerical Mathematics, Wiley-Teubner: New York Stuttgart, 1996.
3. Eriksson K, Estep D, Hansbo P, Johnson C. Introduction to adaptive methods for differential equations. *Acta Numerica 1995*, vol. 4, Iserles A (ed.). Cambridge University Press: Cambridge, 1995; 105–158.
4. Bänsch E. An adaptive finite-element strategy for the three-dimensional time-dependent Navier-Stokes equations. *J. Comput. Appl. Math.* 1991; **36**(1):3–28.
5. Hoffman J, Johnson C. Adaptive finite element methods for incompressible fluid flow. *Error Estimation and Adaptive Discretization Methods in Computational Fluid Dynamics*, *Lecture Notes in Computational Science and Engineering*, vol. 25, Barth TJ, Deconinck H (eds.). Springer-Verlag: Heidelberg, 2003; 97–158.
6. Besier M. Goal-oriented adaptivity in space-time finite element simulations of nonstationary incompressible flows. *Preprint*, Universität Heidelberg 2010.
7. Schmich M. Adaptive finite element methods for computing nonstationary incompressible flows. PhD Thesis, Universität Heidelberg, Heidelberg 2009.
8. Temam R. *Navier-Stokes Equations: Theory and Numerical Analysis*. AMS Chelsea Publishing: Providence, Rhode Island, 2001.
9. Thomée V. *Galerkin Finite Element Methods for Parabolic Problems*, *Springer Series in Computational Mathematics*, vol. 25. Springer-Verlag: Berlin Heidelberg, 1997.
10. Ciarlet PG. *The Finite Element Method for Elliptic Problems*. First edn., North-Holland Publishing Company: Amsterdam New York Oxford, 1987.
11. Girault V, Raviart PA. *Finite Element Methods for Navier-Stokes Equations. Theory and Algorithms*, *Springer Series in Computational Mathematics*, vol. 5. Springer-Verlag: Berlin Heidelberg New York Tokyo, 1986.
12. Hood P, Taylor C. Navier-Stokes equations using mixed interpolation. *Finite Element Methods in Flow Problems*, Oden JT, Zienkiewicz OC, Gallagher RH, Taylor C (eds.), University of Alabama: Huntsville, 1974; 121–132.
13. Brezzi F, Fortin M. *Mixed and Hybrid Finite Element Methods*, *Springer Series in Computational Mathematics*, vol. 15. Springer-Verlag: New York Berlin Heidelberg, 1991.
14. Becker R, Braack M. A modification of the least-squares stabilization for the Stokes equations. *Calcolo* 2001; **38**(4):173–199.
15. Becker R, Braack M. A two-level stabilization scheme for the Navier-Stokes equations. *Numerical Mathematics and Advanced Applications. ENUMATH 2003*, Feistauer M, Dolejší V, Knobloch P, Najzar K (eds.), Springer-Verlag: Heidelberg, 2004; 123–130.
16. dealII. A Finite Element Differential Equations Analysis Library. `http://www.dealii.org/`.
17. Gascoigne. High Performance Adaptive Finite Element Toolkit. `http://www.gascoigne.uni-hd.de/`.

18. Heywood JG, Rannacher R, Turek S. Artificial boundaries and flux and pressure conditions for the incompressible Navier-Stokes equations. *Internat. J. Numer. Methods Fluids* 1996; **22**(5):325–352.
19. Nabh G. On high order methods for the stationary incompressible Navier-Stokes equations. PhD Thesis, Universität Heidelberg, Heidelberg 1998.
20. Heywood JG, Rannacher R. Finite element approximation of the nonstationary Navier-Stokes problem. I: Regularity of solutions and second-order error estimates for spatial discretization. *SIAM J. Numer. Anal.* 1982; **19**(2):275–311.
21. Bristeau MO, Glowinski R, Periaux J. Numerical methods for the Navier-Stokes equations. applications to the simulation of compressible and incompressible viscous flows. *Computer Physics Reports* 1987; **6**(1–6):73–187.
22. Glowinski R. Finite element methods for incompressible viscous flow. *Numerical Methods for Fluids (Part 3)*, *Handbook of Numerical Analysis*, vol. 9, Ciarlet PG, Lions JL (eds.). North Holland: Amsterdam, 2003; 3–1776.
23. Klouček P, Rys FS. Stability of the fractional step θ-scheme for the nonstationary Navier-Stokes equations. *SIAM J. Numer. Anal.* 1994; **31**(5):1312–1335.
24. Turek S. A comparative study of time-stepping techniques for the incompressible Navier-Stokes equations: From fully implicit non-linear schemes to semi-implicit projection methods. *Internat. J. Numer. Methods Fluids* 1996; **22**(10):987–1011.
25. Turek S. *Efficient Solvers for Incompressible Flow Problems. An Algorithmic and Computational Approach*, *Lecture Notes in Computational Science and Engineering*, vol. 6. Springer-Verlag: Berlin Heidelberg, 1999.
26. Kellogg RB, Osborn JE. A regularity result for the Stokes problem in a convex polygon. *J. Funct. Anal.* 1976; **21**(4):397–431.
27. Dauge M. Stationary Stokes and Navier-Stokes systems on two- or three-dimensional domains with corners. Part I: Linearized equations. *SIAM J. Math. Anal.* 1989; **20**(1):74–97.
28. John V. Reference values for drag and lift of a two-dimensional time-dependent flow around a cylinder. *Internat. J. Numer. Methods Fluids* 2004; **44**(7):777–788.